

We are IntechOpen, the world's leading publisher of Open Access books Built by scientists, for scientists

6,900

Open access books available

186,000

International authors and editors

200M

Downloads

Our authors are among the

154

Countries delivered to

TOP 1%

most cited scientists

12.2%

Contributors from top 500 universities



WEB OF SCIENCE™

Selection of our books indexed in the Book Citation Index
in Web of Science™ Core Collection (BKCI)

Interested in publishing with us?
Contact book.department@intechopen.com

Numbers displayed above are based on latest data collected.
For more information visit www.intechopen.com



Ionic Liquids for Green Energy Applications - Local Structure and Dynamics by Advanced Spectroscopic Techniques

Anna Martinelli

Additional information is available at the end of the chapter

<http://dx.doi.org/10.5772/52863>

1. Introduction

Although ionic liquids (ILs) have been known since the beginning of the last century (1814) [1], they are materials of recent advent in the field of green energy applications where their recognition as solvents or electrolytes has ever increased during the last decades.

By definition ILs are molecular salts that melt at low temperatures, *i.e.* around room temperature or below 100 °C [2]. ILs also combine a remarkable set of properties such as high ion density (only ions!), wide temperature ranges of chemical and thermal stability, inflammability and negligible vapor pressure. Hence ILs are particularly suitable for applications where loss to the vapor phase limits the performance or constitutes a hazard, and have therefore been highlighted as the solvents for "green chemistry" in industrial chemical processes [3]. More recently (and as we will see in this chapter), the application of ILs has extended to other fields like electrochemistry, food science and pharmacy [4, 5]. Yet another field of application for ILs is in the metal extraction process from waste water using emulsion ionic liquid membranes, where the IL contributes significantly to the membrane's stability [6].

Typically, an IL consists of an organic cation, such as an imidazolium, pyridinium, pyrrolidinium, or ammonium derivative [7] combined with an organic or an inorganic anion, such as BF_4^- , PF_6^- , CF_3SO_3^- and $(\text{CF}_3\text{SO}_2)_2\text{N}^-$ [8], see Figure 1 for the corresponding molecular structures. Since the discovery of the first IL ($\text{EtNH}_3^+:\text{NO}_3^-$, with melting point at 12 °C [1]), the number of cation–anion combinations has ever increased. In fact, organic cations can essentially be designed with any molecular structure resulting in a huge diversity of possible cation–anion pairs that enables tuning the properties of ILs to suit a particular application.

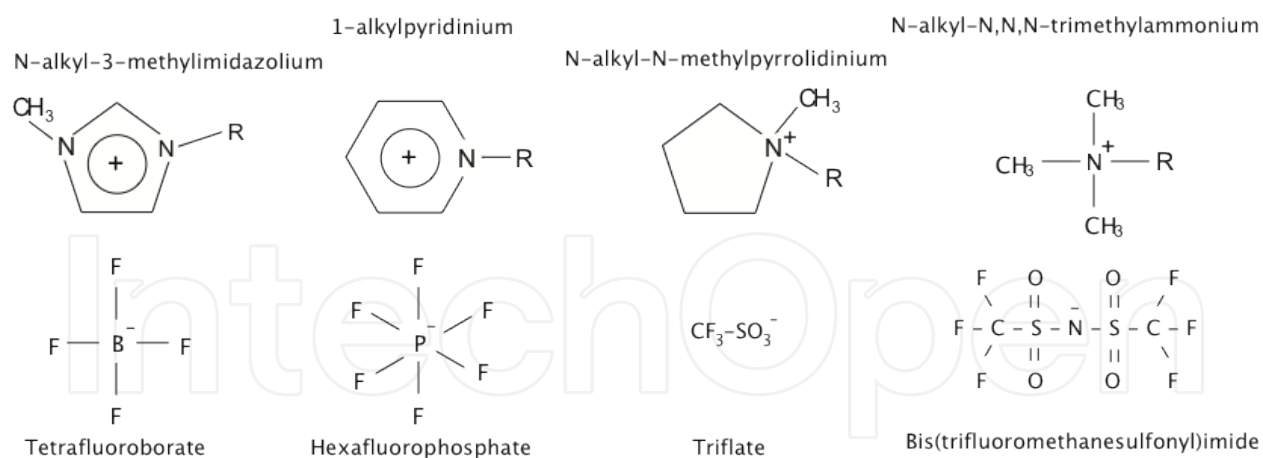


Figure 1. Examples of cation and anion structures typically found in ionic liquids. In these structures, R is the alkylated chain that can be methyl, ethyl, propyl, butyl, etc. In protic ILs R is a proton (H).

Roughly, ILs can be divided into two subgroups: protic (suitable for fuel cells) and aprotic (suitable for lithium batteries and supercapacitors). The former can be obtained through the proton transfer from a Brønsted acid to a Brønsted base (also called neutralization procedure) that, by being a one-step synthesis, results in very pure compounds [8]. The latter can be obtained by the quaternization procedure or the metathesis reaction, which are two-step syntheses involving the exchange of an intermediate anion. Since the intermediate reagents are not always easily eliminated, high-purity can become an issue. The two synthesis procedures to obtain protic and aprotic ILs are also schematically shown in Figure 2. There is a difference between the two types of ILs in the reversibility of the reactions. In protic ILs, for instance, the reaction is theoretically reversible and the completeness of proton transfer can a priori only be predicted by the acid-base pair strength, expressed by the ΔpK_a value.¹ Aprotic ILs, on the other hand, are irreversible compounds. However, apart from this aspect, there is no general difference in the chemico-physical properties between protic and aprotic ILs.

It has been empirically observed that small structural variations on the constituting ions of the ILs have an important influence on the macroscopically observed properties. Understanding these structure-property relationship is therefore key to design new ILs for specific applications. For example, provided a fixed anion, the viscosity and the ionic association degree both increase with the length of the aliphatic chain attached to the cation, which has been related to stronger van der Waals interactions [10]. On the other hand, provided a fixed cation, larger anions result in lower glass transition temperatures, lower melting points, lower viscosities and higher ionic conductivities, which is attributed to a more effective delocalization of the negative charge, hence more loosely coordinating ions [11]. These properties are also strongly affected by the symmetry of the cation and the position of the alkylated substituents on the cationic ring [8]. In protic ILs, it has also been found that provided a fixed anion as for instance the bis(trifluoromethanesulfonyl)imide ($(CF_3SO_2)_2N^-$), smaller cations result in lower glass transition temperatures.

¹ The ΔpK_a is defined as $pK_a^{base} - pK_a^{acid}$ [9].

2. Ionic liquids for energy conversion devices

Because ILs can provide high ionic density, intrinsic ionic conductivity, non-volatility and non-flammability, as well as wide windows of electrochemical stability (up to 5–6 V for certain cation-anion combinations), they represent very interesting materials for applications where transport of ionic species and structural stability are key properties. Concrete examples are electrochemical conversion devices like fuel cells, Li-ion batteries, solar cells and capacitors [12]. In these fields, the ionic conductivity represents a measure of how easily ionic species are transported through the electrolyte. ILs typically display conductivities in the range 10^{-3} – 10^{-2} Scm^{-1} at room temperature and stay liquid in wide temperature ranges extending to several hundreds degrees.²

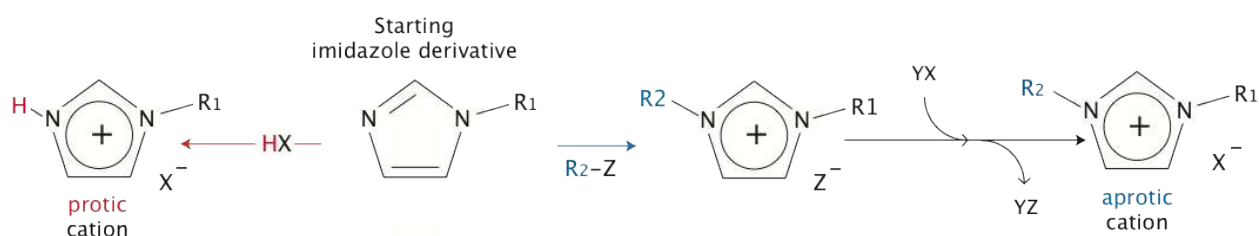


Figure 2. Synthesis procedures for protic ILs by neutralization of a base with an acid (left route, red) and for aprotic ILs by the quaternization method (right route, blue).

As we will see in more detail below (section 5.1) the ionic conductivity in ILs follows a non-Arrhenius dependence on temperature. Compared to the electrolytes conventionally used in for instance commercially available Li-ion batteries, ILs are both safer and greener, which represents an advantage with respect to both environmental and societal issues.

Despite these advantages, the use of ILs in electrochemical devices is limited by their melted state, since leakage can constitute a serious hazard.³ Considerable research efforts are therefore being devoted to find proper ways of confining the ILs into solid-like matrices without, however, sacrificing the ionic conductivity. Proposed confining systems include both polymer based membranes and silica gels, as we will discuss more thoroughly in the next sections.

2.1. Ionic liquids for PEM fuel cells

The operational principles of a low-temperature fuel cell are schematically shown in Figure 3A. The main components in a proton exchange membrane (PEM) fuel cell are the anode, the PEM, and the cathode. The fuel (like H_2 or methanol) is fed at the anode where it is electrochemically split by platinum nano-particles into protons (H^+) and electrons (e^-). The latter follow an external circuit whereas the former diffuse through the PEM towards the cathode.

² Indeed, many ILs decompose before evaporation occurs.

³ Loss of the liquid electrolyte can lead to short circuit and dangerous chemical reactions.

Here, electrons, protons and oxygen recombine to produce water and heat solely. Since the fuel cell does not produce pollutant or in other way hazardous elements, it is considered one of the most promising future devices for clean energy supply.

The archetypical proton conducting material used in low-temperature fuel cells is Nafion, a perfluorinated polymer membrane containing sulfonic acid pending groups ($-\text{SO}_3\text{H}$). Nafion has outstanding chemical and mechanical properties and, upon hydration, separates into hydrophilic and hydrophobic domains of the nano-meter size (see e.g. figure 2 in reference [13]), a structural property that results in well defined channels facilitating the transport of the protonic species (H^+ and H_3O^+). A drawback of Nafion, however, is that at temperatures higher than $80\text{ }^\circ\text{C}$ the membrane dehydrates (due to water evaporation) and drastically loses its conducting properties, see also the conductivity of hydrated Nafion in Figure 3B. Meanwhile, for a realistic implementation of the fuel cell into the transport sector (in e.g. cars and buses) the goal has been set to operate fuel cells at above $120\text{ }^\circ\text{C}$.⁴ At these higher temperatures, electrochemical reactions are faster and less platinum loading is needed at the electrodes, hence the costs of production are also reduced. The challenge today is to find proton conducting materials that are both solid-like (non-leaching) and can provide high enough ionic conductivities (i.e. greater than 10^{-1} Scm^{-1}) at temperatures above $120\text{ }^\circ\text{C}$.

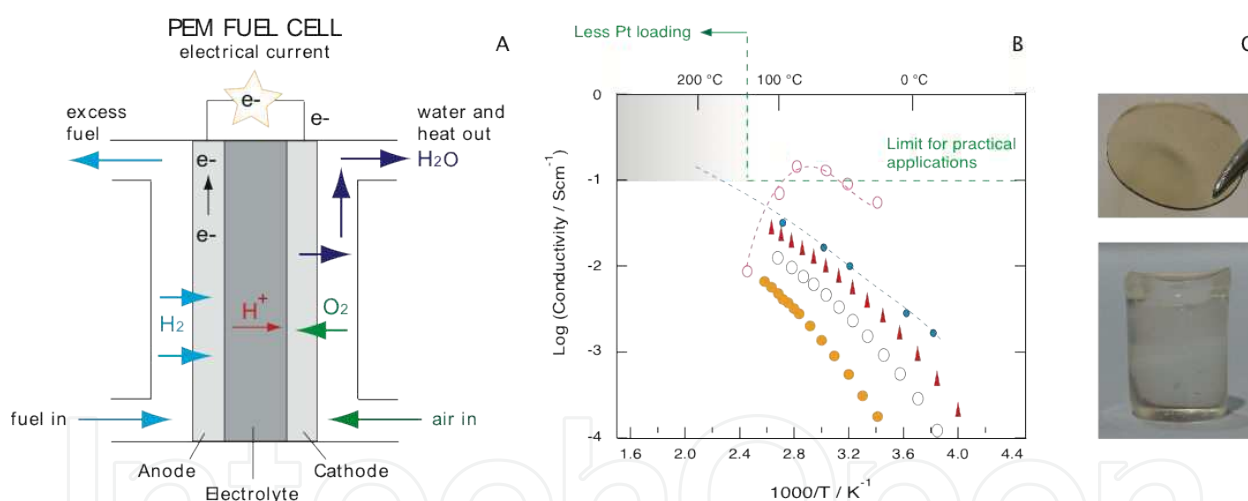


Figure 3. A: schematic of the operational principles in a PEM fuel cell. B: Arrhenius plot of ionic conductivities for diverse PEM fuel cell electrolytes: 80EIM:20PVdF (in wt%, \circ), 80PMP/HTFSI:20PVdF (in wt%, Δ), and 40TFTEA:20Nafion (in wt%, \bullet); an ion gel (\blacklozenge); and hydrated Nafion (\circ). Here, EIM is ethylimidazoliumbis(trifluoromethanesulfonyl)imide, PMP is N-propyl-3-methylpyridinium bis(trifluoromethanesulfonyl)imide, and MSTEA is methane sulfonatetriethylammonium. Data points have been reproduced with permission from references [14, 15, 16]. The shadowed area shows the target set by the U.S. DOE for next-generation proton conducting materials (see also footnote 4). C: a photo of an IL swelled PVdF based membrane (top) and of an ionogel of the $\text{C}_6\text{mimTFSI}$ (bottom).

⁴ In the Multi-Years Development Program of the U.S. Department of Energy (DOE) for the Fuel Cell Technology the requirement for next-generation proton exchange membrane (PEM) electrolytes is ($\geq 10^{-1}\text{ Scm}^{-1}$ at temperatures above $120\text{ }^\circ\text{C}$). Achieving this goal will facilitate the implementation of the fuel cell into the transport sector (buses, cars, scooters, etc).

Because ILs have a high ionic density, an intrinsically high ionic conductivity and are non-volatile, they are considered suitable materials to replace the concept of hydrated Nafion membranes in fuel cell applications. One investigated approach in this direction has been the swelling of PVdF-based polymer membranes by aprotic ILs of the methylpyridinium or propylimidazolium cation and the bis(trifluoromethanesulfonyl)imide (TFSI) anion [14], see also Figure 3C (top). However, to provide the protonic species a chemically compatible acid had to be included, more specifically HTFSI. Swelling the membrane with a protic IL instead resulted in a simpler system since the protic species were intrinsically provided by the (protonated) cation of the IL [15]. The IL-swelled polymer membrane concept results in reasonable ionic conductivities, however at the expense of poor mechanical stability. Nafion membranes swelled with protic ILs of the triethylammonium cation and the methane sulfonate (CH_3SO_3^-) or triflate (CF_3SO_3^-) anion is an alternative and more recent concept of proton exchange membranes [16]. This type of electrolytes show a smaller loss in conductivity with respect to the bulk IL and also better mechanical resistance than PVdF based membranes. In addition, these ammonium based ILs display a range of different degrees of cation:anion dissociation and an ability for proton exchange that also contribute to higher conductivities [17].

The ionic conductivities of these IL swelled polymer membranes are compared on a common Arrhenius plot in Figure 3B, together with the conductivity of hydrated Nafion. The reader may note that the shadowed area, representing the target set by the U.S. DOE (see footnote 4), is still not hit, implying that further scientific efforts are needed to develop new materials able to meet the set requirements.

2.2. Ionic liquids for Li-ion batteries

The most modern Li-ion battery is based on the rocking chair electrode model and the intercalation of Li ions into and from the electrodes [18]. In this battery concept the anode is typically carbonaceous (*e.g.* graphite) while the cathode consists in a layered oxide (*e.g.* LiCoO_2), a polyanion (*e.g.* LiFePO_4) or a spinel (*e.g.* LiMnO_2), and the electrolyte is typically a Li-salt (*e.g.* LiPF_6 or LiBF_4) dissolved in an organic solvent like ethylene carbonate (EC) or propylene carbonate (PC). The operational principles of a conventional Li-ion battery are shown in Figure 4A. The main issue with this battery concept concerns safety, which slows down the implementation of large-scale cells for energy storage and vehicle applications. Unpredictable events like short circuits or local overheating can trigger undesired reaction between battery components and the liquid organic electrolyte that can develop in drastic local heating and, eventually, into fire or explosion. Therefore, the replacement of conventional organic solvents with ILs, represents a huge improvement in terms of safety, the major advantages with this respect being non-volatility and non-flammability. In addition, the solubility of lithium salts (*e.g.* LiBF_4 or LiTFSI) in ILs is very high, and comparable to that of organic polar solvents. Different IL structures for Li-ion battery applications are under investigation in many industrial and academic laboratories, the electrochemical stability towards the electrodes being one main issue to solve. However, for an improved battery performance the growing of the surface electrode interface (SEI) must also be given further attention.

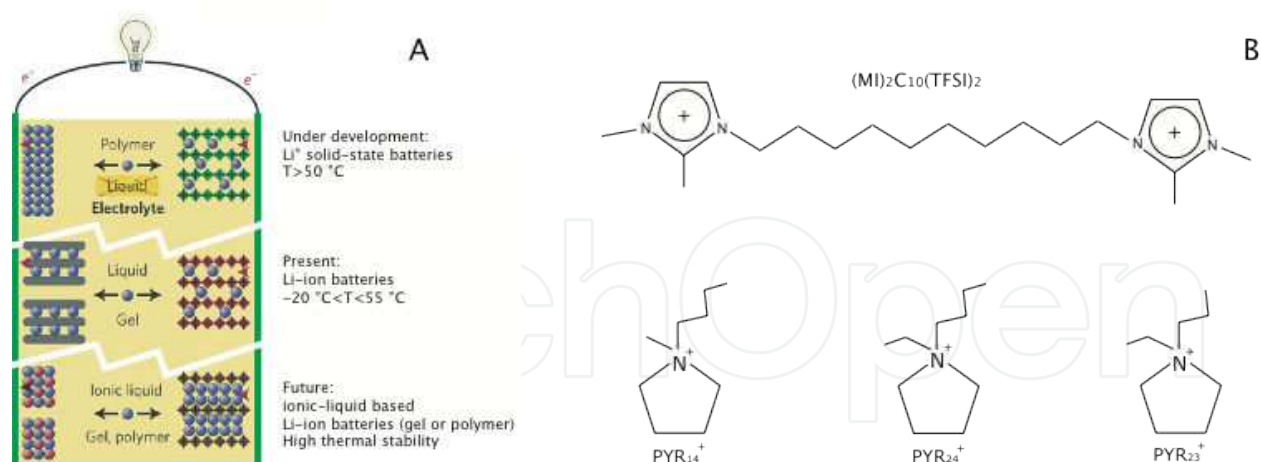


Figure 4. A: schematic of under development, present, and future lithium battery concepts, including those based on ILs as electrolytes (reproduced with permission from reference [5]). B: some cationic structures of interest for use in Li-ion batteries, a dicationic imidazolium based (top) and three pyrrolidinium derivatives (bottom), respectively.

The most investigated family of ILs for Li-ion battery application is that of the pyrrolidinium cation (Pyr), which has shown a better stability in time towards lithium metal electrodes than the previously investigated imidazolium based systems, and a wider electrochemical stability window [19]. Also, TFSI⁻ results in low-melting ILs and high conductivities in combinations with many cationic structures due to the high charge delocalization and is therefore also the most used and investigated anion. To achieve chemical compatibility, the lithium salt most commonly dissolved in these ILs is consequently the LiTFSI. Thus, the typical IL based electrolyte for Li-ion battery applications is LiTFSI-Pyr_xTFSI, where x and y are alkyl chains of variable length, see also Figure 4B. Nevertheless, as we will discuss in more details below, even small structural variations on the Pyr cation can result in different properties, like different phase behavior and dependence on temperature of the ionic conductivity.

2.3. Ionogels

Ionogels constitute a very recent material concept based on the nano-confinement of ILs into silica; see Figure 3C (bottom) for a photo of an ionogel prepared in our laboratories. Compared to IL swelled polymer membranes, ionogels can incorporate a considerably higher volume of liquid (up to 98%) without loosing in mechanical resistance [20, 21]. Ionogels can be prepared through a sol-gel synthesis that follows a non-aqueous route proposed by K. G. Sharp [22], consisting in the reaction of tetramethylorthosilicate (TMOS) with formic acid (FA). During this reaction, nano-sized particles of silica (SiO₂) are formed that first undergo aggregation and then gelation. If the sol-gel reaction is let occurring inside an IL as a co-solvent, the final gel will be three-dimensionally interpenetrated by the IL.

Recent results from magic angle spinning ¹H NMR experiments have shown that even at high degrees of nano-confinement⁵ the dynamical properties of the IL are only marginally slowed down [23, 24]. Thus, ionogels represent an elegant route to robust and non-leaching

⁵ Or low ionic liquid contents in the ionogel.

nano-structured electrolytes. So far, the ILs used in the synthesis of ionogels have primarily included 1-ethyl-3-methyl imidazolium ($C_2\text{mim}$) or 1-butyl-3-methyl imidazolium ($C_4\text{mim}$) cations, whose ionic conductivity is shown in Figure 3B together with those of hydrated Nafion and IL swelled polymer membranes. From this plot it is evident that the ionogel concept has the potentiality to meet the requirements in terms of high conductivity at temperatures higher than 120 °C, as set by the U.S. DOE.

In our laboratories we are currently investigating the use of the 1-hexyl-3-methyl imidazolium ($C_6\text{mim}$) cation, which has a longer alkyl side chain and may thus induce interesting structural features in the gel. We have indeed found by time resolved Raman and ^1H NMR spectroscopy that a structural reorientation of the cation may occur in concomitance with the sol-gel transition [25], which may also be accompanied by a local cation-anion reorganization.⁶ We are undertaking detailed structural investigations at the molecular level since this understanding will guide the design of next-generation ionogels tailor made for specific applications. To be suitable for fuel cell applications, for instance, ionogels must be prepared with protic ILs, whereas to be used in Li-ion battery applications, a suitable Li salt-IL should be used in the sol-gel synthesis. To the best of our knowledge, none of these approaches have been reported so far and, in our laboratories, efforts will be primarily spent on the former.

3. Structural investigations

The local structure is one hot issue in the field of ILs, where recent progresses have mainly concerned the understanding of the mesoscopic segregation in the liquid state. With local in this context we mean the nm or molecular scale range, where effects of conformational evolution, crystalline-to-amorphous transitions, ionic clustering *etc* occur. Experimental techniques that have been successfully used to resolve this size domain are vibrational (Raman and infrared) spectroscopy, solid state Nuclear Magnetic Resonance (NMR) spectroscopy and Small Angle X-ray Scattering (SAXS), which will also be discussed in the sections that follow. Knowing the local organization of cations and anions in ILs is very important, in particular because the resulting ion-ion association can in turn have an impact on the ionic transport properties. The reader should recall that ILs are only comprised of ions, that the inter-ionic electrostatic forces are very important and that, as a consequence, anions and cations should be considered as structurally and dynamically associated pairs.

A particular structural feature can also affect the electrochemical performance of the IL. For instance, it has been found that in aprotic ILs based on the 1-ethyl-3-methylimidazolium ($C_2\text{mim}$) cation the substitution of the acidic proton on the ring (position C_2) by an alkyl chain decreases the reduction potential [27], which is otherwise too large for practical applications in Li-ion batteries. Also, the addition of a Li-salt to ILs results in ionic clustering and consequently a reduced number of free charges, as also discussed in section 4.1 and reference [28].

⁶ From ongoing analysis of confocal μ -Raman/x-ray (small angle x-ray scattering, SAXS) data collected at the ID13 beam line of the ESRF facility in Grenoble [26].

3.1. Raman spectroscopy: Conformational isomerism

Vibrational spectroscopy (including Raman, infrared, neutron and luminescence spectroscopy) is a powerful technique to investigate the structure in materials on a molecular or smaller level. More specifically, issues like dissociation, inter-molecular interactions, crystallinity and conformations can be investigated in both the liquid and solid state. In this section however, only Raman spectroscopy will be treated.

The basic principle of Raman spectroscopy⁷ is the excitation of the material by monochromatic light with wavelength usually in the visible range⁸ and the collection of the inelastically scattered light. The latter contains detailed information on the molecular vibrations characteristic of the investigated material. If the energy of the incident light is $h\omega_0$, a minor part of this ($\sim 10^{-6}$) will be inelastically scattered (or Raman scattered) with a gain or loss in energy. The inelastically scattered light has energy $h\omega_0 \pm h\omega_{\text{vib}}$, where $h\omega_{\text{vib}}$ is the vibrational energy exchanged in the scattering process. The plus/minus signs correspond to anti-Stokes and Stokes scattering respectively, see Figure 5A. In the simplest classical treatment, where atoms are treated as particles bound by weightless springs and vibrate around their equilibrium position, the vibrational frequency can be described as

$$\omega_{\text{vib}} \propto \sqrt{\frac{k}{M}} \quad (1)$$

where k is the bond strength and M the reduced mass of the oscillating system.⁹ From this expression it follows that molecules with atoms of different masses and bond strengths will have distinct fingerprints in a Raman spectrum, where Raman intensity is plotted versus frequency of vibration (expressed in cm^{-1}). As a consequence, changes in the dissociation state, in the closest chemical environment, or in the internal bond rotations can be studied analyzing intensity and frequency shifts of the vibrational modes.

The conformation adopted by cations and anions in ILs has been one such investigated structural feature. This is of interest since the relative orientation of the cation-anion pair can in turn affect the association degree of the ions and thus the dynamical properties of the IL. The TFSI anion, for instance, can adopt two different conformations, the *cisoid* (or C_1) and the *transoid* (or C_2) that differ in the orientation of the $-\text{CF}_3$ groups with respect to the internal S-N-S bond, see Figure 5B. The fingerprints of these two conformations were first theoretically predicted to be found in the low-frequency spectral range $260\text{--}370 \text{ cm}^{-1}$ [31] and then also experimentally distinguished for protic and aprotic ILs of the imidazolium, pyridinium and pyrrolidinium cations [29]. This study shows that as the temperature is increased the population of *cisoid* conformers increases¹⁰ (see also Figure 5C) and that the enthalpy of conforma-

7 A more thorough description of the Raman spectroscopy technique can be found in reference [30].

8 Nevertheless, laser light in the UV and near IR range can also be used.

9 In a two-atoms system with masses m_1 and m_2 the reduced mass M is defined as $(m_1 m_2)/(m_1+m_2)$.

10 The *transoid* is indeed the conformation most stable at low temperatures and commonly found in the crystalline phase.

tional change, ΔH , also varies with the structure of the associated cation. Moreover, it seems from recent investigation of ionogels prepared with the IL C_1C_6TFSI , that nano-confinement in silica also can increase the population of the C_1 conformers [25]. So, it is clear that even very small changes on the cationic structure can induce important effects on the anion's conformation. In this respect, J.D. Holbrey *et al.* have reported the unusual *cisoid* conformation for $TFSI^-$ in the solid-state structure for the case of the 1,3-dimethylimidazolium cation [32], as opposed to what is found with the 1,2,3- triethylimidazolium cation and most other investigated imidazolium-based ILs (that adopt the *transoid* form in the solid-state).

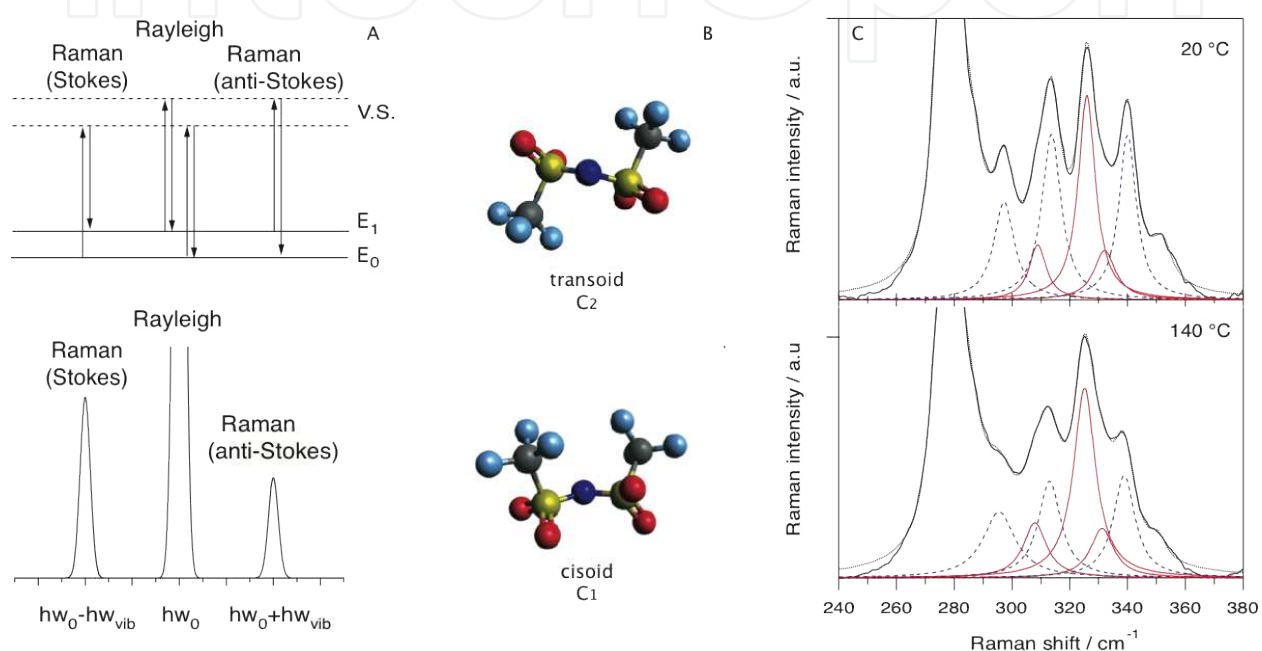


Figure 5. A: the inelastic scattering process during a Raman experiment with Stokes lines corresponding to energy loss and anti-Stokes to energy gain, respectively. The Rayleigh lines correspond to no energy exchange. B: the two conformations in which the TFSI anion can be found in, *i.e.* the *cisoid* (or C_1 , bottom) and the *transoid* (or C_2 , top). C: Deconvolution of Raman spectra recorded at different temperatures for the protic IL EIMTFSI (ethylimidazolium bis(trifluoromethanesulfonyl)imide). The fitting (Lorentzian) components corresponding to the *cisoid* and *transoid* contributions are shown in red (solid line) and blue (dashed line), respectively. These Raman spectra are reproduced with permission from reference [29].

Also the conformational isomerism of cations can be investigated by vibrational spectroscopy, as for instance demonstrated in reference [33]. The number of conformations in cations can be significantly increased when long alkyl side chains are attached, due to a larger degree of rotational freedom around the C-C bonds and the orientation of the chain with respect to the cationic head. For the case of 1-butyl-3-methylimidazolium tetrafluoroborate (C_4mimBF_4) the coexistence of at least four conformers was found, GG, GA, TA and AA, with the population of the most stable GA and AA increasing as temperature is decreased [33].

Raman spectroscopy has also greatly contributed to understand the formation of larger ionic aggregates, or $[Li(TFSI)_n]^{-(n-1)}$ clusters, upon addition of LiTFSI to ILs of the pyrrolydinium

cation. In reference [28], the authors discuss possible types of $[\text{Li}(\text{TFSI})_n]^{-(n-1)}$ aggregates in ILs of different cations, *i.e.* pyrrolidinium and imidazolium, the latter both in the mono- and di-cationic form, analyzing the TFSI-characteristic Raman mode at $\sim 740 \text{ cm}^{-1}$. This study shows that for all ILs the number of TFSI anions strongly coordinating to one Li-ion drastically increases at very low salt concentrations, where values of n in the range 4–6 dominate. For intermediate LiTFSI concentrations, triplets of the type $[\text{Li}(\text{TFSI})_2]^-$ are found instead. It is interesting to note that these different coordination regimes also correspond to different strengths of TFSI:Li-ion interaction, which in turn affect the macroscopically observed ionic conductivity (see also Figure 3 in reference [28] and the discussion therein).

3.2. NMR spectroscopy: Heteronuclear coupling

Nuclear magnetic resonance (NMR) is a phenomenon based on the exchange of electromagnetic radiation when magnetic nuclei are exposed to a magnetic field. A requisite for this phenomenon is that the nuclei have non-zero spins, which applies for all isotopes with an odd number of protons and/or neutrons. A key feature in NMR spectroscopy is that the resonance frequency of a particular nucleus is directly proportional to the strength of the applied field and to the magnetic properties of the nucleus itself. The basic relation is thus:

$$\omega_0 = \gamma \cdot B_0 \quad (2)$$

where ω_0 is the precession frequency of the nucleus, B_0 is the externally applied magnetic field, and γ_0 is the gyromagnetic ratio characteristic of the investigated nucleus. It might appear from this relation that all nuclei having the same γ_0 would resonate at the same frequency. This is not the case since the most important perturbation of the NMR frequency is the 'shielding' effect of the surrounding electrons. The rotation of these electrons produces a spin, which results in a magnetic field that counteracts the magnetic field of the nucleus. In general, this electronic shielding reduces the resonance frequency, whereby same nuclei found in different molecular structures can be resolved by their characteristic chemical shift (δ , expressed in ppm).

By using different types of pulse sequences, where the pulses vary in shape, frequency and duration, dynamical or structural information can be extracted from an NMR experiment. Multi-dimensional NMR spectroscopy is a kind of Fourier Transformed (FT) NMR that allows detecting nuclear-nuclear interactions through magnetization transfer. Through-bond and through-space interactions can be detected, the latter in particular allowing to establish distances between atoms (*e.g.* by 2D-FT NMR). Although widely used to investigate proteins and crystalline materials, NMR spectroscopy has scarcely been used to elucidate the local structure in ILs. Of great potentiality in this context are heteronuclear and cross-polarization (CP) MAS NMR experiments, the latter being particularly suitable where the IL phase is present in a solid-like matrix, as in a gel or in a polymer.

One of the exceptions is the study reported in reference [17], where the structure and local organization in protic ILs of the triethylammonium (TEA) cation have been elucidated by

combining 1- and 2D heteronuclear NMR experiments The authors show that the choice of different TEA⁻ anionic species pairs strongly affects the dissociation scheme:



where A⁻ denotes the anion. These experiments also evidence the coupling between the dissociation state of the proton in the IL and the diffusive behaviors of the individual ionic species (see also Table 1 in reference [17]). For instance, even though in TEA-TFSI the ions are fully dissociated the proton diffuses with the cation and faster than the TFSI anion, whereas in the IL TEA-acetate the proton is fully dissociated from the cation, and is also the fastest diffusing species. These observations have obvious implications for practical use in fuel cells where the transport of the protic species through the electrolyte and its reactivity at the cathode are key properties.

3.3. SAXS: Nano-segregation

Along with a peculiar set of physico-chemical properties, ILs also show a complex local organization with self-aggregating polar and non-polar domains of the nanometer size. This mesoscopic separation was first predicted by molecular dynamic (MD) simulations and later also experimentally confirmed by small (and wide) angle x-ray scattering measurements (SAXS (and WAXS)). Before discussing in detail these results, the basic principles of an x-ray scattering experiment will be briefly explained.

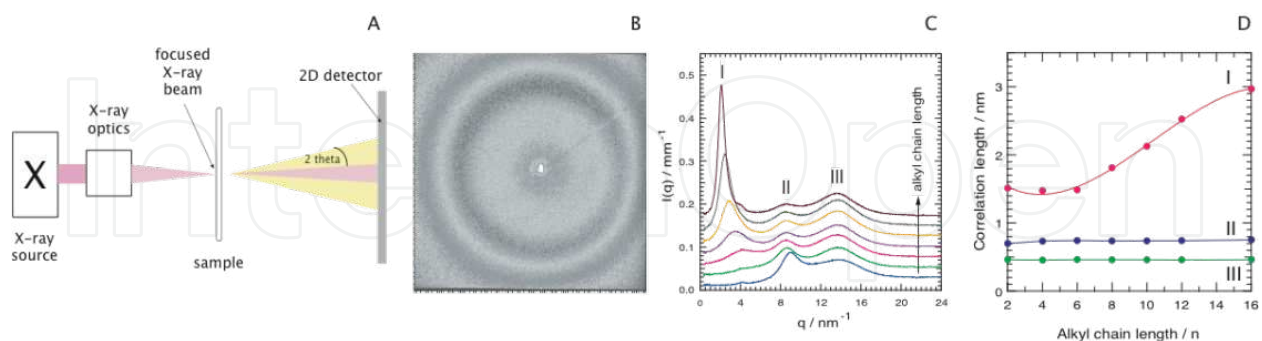


Figure 6. A: Schematic of a SAXS experimental set up. B: a typical 2D diffraction pattern recorded for IL containing samples [26]. C: the 2D diffraction pattern recorded for 1-alkyl-3-methylimidazoliumTFSI ILs transformed into intensity, I, as function of scattering vector, q [37]. D: correlation lengths derived from the diffraction pattern in C using $d=2\pi/q$.

In a SAXS experiment the sample is exposed to x-ray radiation with wavelength in the range of a few Å, and the elastically scattered x-rays are recorded at low angles, typically close to 0°, Figure 6A. In the presence of structural inhomogeneities in the nm range, a diffraction pattern is recorded if the following condition is fulfilled (Bragg's law):

$$n\lambda = 2d\sin(\theta) \quad (4)$$

where λ is the wavelength of the incoming x-ray, d is the repeat distance of the local structure, and θ the angle at which diffraction peaks are collected. Unoriented samples yield a centro-symmetric pattern on a 2D detector (Figure 6B), which is radially averaged to give the typical plots of diffracted intensity versus scattering vector q (Figure 6C). Since the scattering vector q is defined as:

$$q = (4\pi / \lambda) \sin\theta \quad (5)$$

the real space correlation length d can be experimentally estimated as $d=2\pi/q$, see also Figure 6D.

The intriguing property of ILs is that even in the liquid state they can display clear scattering peaks in the x-ray diffraction pattern. This feature has been repeatedly reported by several authors and for diverse cation-anion combinations. The first studies focused primarily on ILs of the imidazolium cations [34], but more recent investigations have extended to those of ammonium and pyrrolidinium derivatives also, associated with PF_6^- , BF_4^- , Cl^- or TFSI⁻ [35]. SAXS (and WAXS) diffraction patterns show that the low- q feature (corresponding to long real space distances) increases in intensity and shifts to lower values as the length of the alkyl side chain on the cation increases. This behavior is now rationalized as the separation of non-polar domains (consisting of aggregated alkyl side chains) from the polar matrix composed of anions and cationic head groups. This model can be compared to the micelle-like structuring occurring in n -alcohols [36].

As shown in Figure 6C, a typical SAXS diffraction pattern recorded for 1-alkyl-3-methylimidazolium TFSI ILs, and covering the wide q -range 0.2–30 nm⁻¹, displays three peaks attributed to cation-cation (0–5 nm⁻¹), anion-anion (5–11 nm⁻¹) and intramolecular (12–16 nm⁻¹) correlations. This IL series includes cations with the alkyl chain varying from ethyl ($n=2$) to hexadecyl ($n=16$) [37]. In this context the reader should know that the central peak is relatively strong for the TFSI anions but can be much less intense for smaller anions like Cl^- or Br^- . In agreement with previous results we also record an increasing intensity for the cation-cation correlation length upon longer alkyl chains; however, by including very long chains in the investigated series we also evidence a non-strictly linear dependence of the corresponding correlation length d , Figure 6D [37]. For ILs where the alkyl chain is an octyl or shorter ($n \leq 8$) a linear dependence has previously been assumed, whereas our results point to a deviation for longer chains. Since we have independently also found a non-linear dependence on n for the cationic hydrodynamic radius extrapolated from self-diffusion meas-

measurements ($r_+(n) = kT/c\pi\eta D_+(n)$), we believe that this non-linearity reflects a certain degree of inter-digitation of the alkyl chains, previously not believed to occur for shorter alkyl chains.

This finding fits well into the vivid debate currently ongoing on the true interpretation of the SAXS patterns: some researchers believing in a real mesoscopic separation as several times evidenced by SAXS and WAXS experiments [38], and other claiming that the observed diffraction pattern only reflects the internal structural inhomogeneity of the cation with no implications of a long-range ordering [39]. The main point of our study [37], however, is the correlation experimentally found between the transport properties (from pfg-NMR measurements) and the local ordering (from SAXS data) of the individual ionic species. In particular, we have found that there is a correlation between the dispersion curves of the anion-anion and cation-cation correlations and the measured self-diffusion constants independently measured for anions (D_-) and cations (D_+) in the ILs (see also Figure 8B and the thorough discussion in reference [37]).

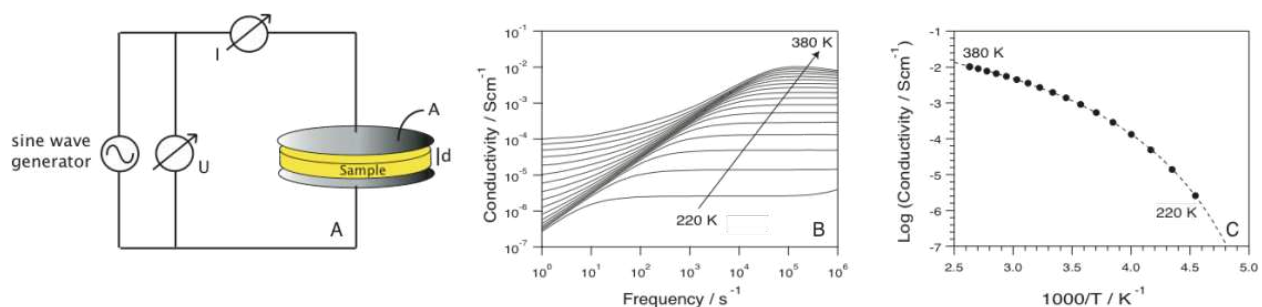


Figure 7. A: Schematic picture of the experimental set up for a dielectric spectroscopic measurement. Sample thickness, d , and surface area, A , are indicated in the figure. B: Conductivity–frequency plot for the protic ionic liquid N-ethylimidazolium bis(trifluoromethanesulfonyl)imide (EIMTFSI). C: Temperature dependence of conductivity, extrapolated from the constant plateau in B.

4. Dynamical investigations

When ILs are used as electrolytes in energy conversion devices like fuel cells or Li-ion batteries, they have the two-fold functionality to separate the electrodes (and thus prevent from short circuit) and to be the conducting medium for the electro-active ionic species (H^+ or protic species in PEM fuel cells, and Li^+ in Li-ion batteries). It is therefore of great interest to investigate and understand the transport properties in ILs, in particular the ionic conductivity and the self-diffusion of ionic species, but also transport phenomena under operational conditions that could lead to concentration gradients of the electrolyte (*e.g.* due to electro-osmotic drag). The most common techniques to investigate these phenomena, as well as recent important results, are presented and discussed in the following sections.

4.1. Dielectric spectroscopy: Ionic conductivity

Dielectric spectroscopy can be used to measure the ionic conductivity in diverse materials, including liquids. In such a dielectric experiment, the sample is sandwiched between two electrodes of surface area A and separation d , as shown in Figure 7A. This corresponds to a parallel plate capacitor, with capacitance C defined by

$$C = \epsilon_0 \epsilon \frac{A}{d} \quad (6)$$

where ϵ_0 is the dielectric constant in vacuum and ϵ is the frequency-dependent complex dielectric function of the material, $\epsilon(f)$. In the dielectric experiment, an alternating voltage (U) is applied to the electrodes and the resulting alternating current (I) is measured. These quantities are related through the complex impedance (Z) of the material, *i.e.* $Z=U/I$. The complex impedance is in turn related to the dielectric function of the material through the relation

$$\epsilon = \epsilon'(f) - i\epsilon''(f) = -\frac{i}{2\pi f C_0 Z} \quad (7)$$

where C_0 is the empty cell capacitance. In Eq. 7, $\epsilon'(f)$ and $\epsilon''(f)$ are the real and imaginary parts of the dielectric function $\epsilon(f)$. The dependence of ϵ on frequency, f , and temperature, T , is typically investigated in the experiments. The presence of mobile charges in a material results in conductivity, which can be obtained in a dielectric experiment from the dielectric function through the relation:

$$\epsilon''(f) = \frac{\sigma'(f)}{2\pi f C_0 \epsilon_0} \quad (8)$$

This equation shows that the real part of conductivity contributes to the imaginary part of the dielectric constant. Thus, because of the f^{-1} dependence in Eq. 8, in the plot of $\epsilon''(f)$ the dc conductivity will contribute as a rapidly increasing signal at low frequencies. The dc-conductivity can be directly investigated in a frequency plot ($\sigma(f)$), as shown in Figure 7B, and is extrapolated from the constant plateau, which moves to lower frequencies as temperature is decreased. At lower frequencies, the decay in conductivity is due to polarization effects at the electrodes. This occurs when the conductivity of the material is appreciable and a high charge density is created at the surface of the electrodes [40, 41]. In Figure 7C, the temperature dependence of the dc conductivity of the IL ethylimidazolium-bis(trifluoromethanesulfonyl)imide (EIMTFSI) is shown. This plot shows the typical non-Arrhenius dependence of conductivity on temperature observed for all ILs in their melted state. Instead, the conductivity data are very well described by the Vogel-Fulcher-Tamman (VFT) equation

$$\sigma = \sigma_0 e^{-\frac{B}{T-T_0}} \quad (9)$$

where σ_0 is the ionic conductivity at very high temperatures ($T \gg T_0$), B is a constant related to fragility (commonly discussed in glass-forming liquids) and T_0 is the ideal glass transition temperature. If compared on the same plot, ILs with larger values of B will display less curved conductivity data sets, similarly to what is observed when plotting viscosity as a function of inverse temperature. In our recent investigation of a large series of 1-alkyl-3-methylimidazolium ILs of the TFSI anions [37], we have extrapolated B values by fitting the conductivity data with a VFT equation. These values are also given in Table 1, indicating that for longer alkyl chains attached to the cation the IL becomes progressively less fragile (or stronger, larger B values). This is in agreement with that the cation-anion association also becomes more important, as also shown by the trend of $\Lambda_{\text{imp}}/\Lambda_{\text{NMR}}$ (also given in Table 1).

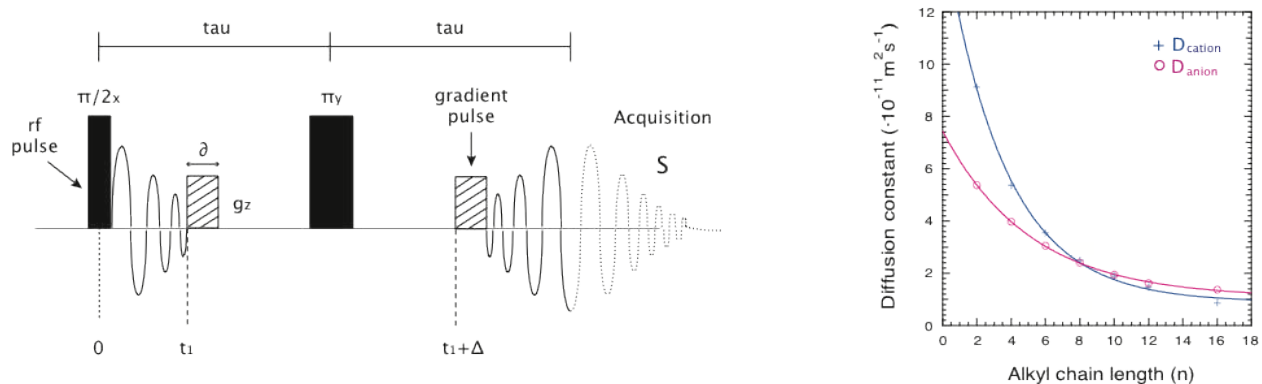


Figure 8. A: Schematic of the most basic pfg-NMR pulse sequence for diffusion experiments (reproduced with permission from reference [44]). B: Self-diffusion constants of the anions (pink) and cations (blue) in 1-alkyl-3-methylimidazolium TFSI ILs, for increasing alkyl chain lengths (see also reference [37]).

In our laboratories we have found that if the ionic conductivity of ILs is plotted as a function of T_g/T , where T_g is the experimentally found glass transition temperature, data fall onto master curves [42, 43]. This universal behavior resulting from T_g -scaling is a strong indication that conductivity is dominated by the viscous properties in the whole temperature range investigated.¹¹ Further, we have found that ILs of the same cationic structure but doped with different amounts of Li-TFSI also fall onto master plots through this scaling. However, even small structural changes on the cation in terms of, for instance, alkyl chain length can result in different B values, and therefore different curvatures, also in a T_g -scaled plot (compare for example the case of Pyr₁₄ with Pyr₂₄ in reference [42]).

¹¹ Since viscosity is a quantity strongly related to the glass transition temperature T_g .

4.2. NMR spectroscopy: Self-diffusion

A very powerful tool to study the dynamics of ionic species in liquid materials is by pulsed field gradient nuclear magnetic resonance (pfg-NMR) spectroscopy. This technique measures the translational diffusion of molecules in time scales larger than milliseconds.

The most basic pfg (or Stejskal and Tanner 1967) pulse sequence used to estimate self-diffusion constants is schematically shown in Figure 8A. This consists of a spin-echo experiment with the 180° pulse in between two equal gradient pulses of magnitude g_z and duration δ . The first field gradient pulse introduces a dephasing in the precession frequency and the second pulse partially refocuses the phases. The phase difference due to the diffusing spins that cannot recover the initial phase leads to the attenuation of the NMR echo, while the signal loss in the case of unrestricted diffusion is proportional to the average root mean square displacement occurring between the two gradient pulses.

Typically, the magnetic field gradient g_z is imposed along the z-direction (that is also the direction of the static field, see B_0 in Eq. (2)) and, as a consequence, the Larmor frequency of a spin becomes a position label (from the NMR basic relation $\omega = \gamma B$).¹² If the duration between the leading edges of the gradient pulses is denoted Δ , the duration and the strength of the gradient field δ and g , the attenuation of the echo signal is described by

$$I = I_0 e^{-(\gamma^2 g^2 D \delta^2)(\Delta - \delta/3)} \quad (10)$$

From this relation the self-diffusion constant D of the diffusing species can be extrapolated. Typical self-diffusion constants at room temperature in ILs are found in the range 10^{-10} - 10^{-11} m^2s^{-1} , as also given in Table 1 for ILs of the imidazolium cation and the TFSI anion [45]. These values show that D tend to decrease with the length of the alkyl chain on the imidazolium, which is a direct effect of increased viscosity (η) and, in theory, also of the ionic size (r_s). Indeed, these quantities are closely related through the Stokes-Einstein relation

$$D = kT / 6\pi\eta r_s \quad (11)$$

Where k is the Boltzmann's constant, T is the temperature, and r_s the hydrodynamic (or Stokes) radius. Currently a vivid debate is ongoing on whether, and to what extent, Eq. 11 is valid for ILs. In fact, not always do larger molecules display the lowest D values [46], and in some IL systems the fractional form of the $D(\eta)$ dependence has found to be more appropriate:

$$D \propto (T/\eta)^\beta \quad (12)$$

¹² Where ω is the Larmor frequency (radians s^{-1}), γ the gyromagnetic ratio ($\text{rad T}^{-1}\text{s}^{-1}$) and B is the strength of the magnetic field (T).

For the few ILs investigated through the fractional form of the Stokes-Einstein equation, β has found to be less than unity and in the range 0.92–0.95 [47, 48]. These observations indicate that ILs cannot always be treated as classical hydrodynamic systems, and that a complex combination of solvating and electrostatic forces govern the self-diffusion of the molecular species.

Another interesting aspect of pfg-NMR measurements is that the molar conductivity (Λ_{NMR}) can be calculated from the self-diffusion constants using the Nernst-Einstein equation¹³

$$\Lambda_{\text{NMR}} = N_A e^2 (D_+ + D_-) / kT \quad (13)$$

In electrolytic systems this quantity becomes interesting if compared to the molar conductivity directly measured by impedance spectroscopy (Λ_{imp} , see section 5.1). The molar conductivity ratio $\Lambda_{\text{imp}}/\Lambda_{\text{NMR}}$ illustrates well the degree of cation-anion aggregation in ILs at equilibrium and represents a measure of the tendency to form higher ionic complexes, as opposed to completely dissociated systems. Indeed, while impedance measurements record the displacement of charged species only, pfg-NMR measurements record the movement of all probed molecules regardless their charged state (or ionic complexation). As a representative case, values for the $\Lambda_{\text{imp}}/\Lambda_{\text{NMR}}$ ratio in ILs of the imidazolium cation are given in Table 1. These are all smaller than one indicating that not all the diffusing species in the IL contribute to the ionic conduction, *i.e.* ionic aggregates and/or clusters are formed [45]. In addition, the trend for $\Lambda_{\text{imp}}/\Lambda_{\text{NMR}}$ indicates that for longer alkyl chains the cation-anion association also becomes stronger. Table 1 also illustrates that cations and anions do not always have the same diffusivity, even though this discrepancy becomes smaller for longer alkyl chains. We have recently addressed this specific issue by combining SAXS and pfg-NMR experiments on a large series of 1-alkyl-3-methylimidazoliumTFSI ILs [37].

Structure of cation	$\Lambda_{\text{imp}}/\Lambda_{\text{NMR}}$ [45]	B_{imp} [37]	$D_{\text{NMR}+}$ [45] ($\cdot 10^{-11} \text{ m}^2 \text{ s}^{-1}$)	$D_{\text{NMR}-}$ [45] ($\cdot 10^{-11} \text{ m}^2 \text{ s}^{-1}$)
C ₁ mim	0.76	n.a.	5.8	3.3
C ₂ mim	0.75	627	6.2	3.7
C ₄ mim	0.61	772	3.4	2.6
C ₆ mim	0.57	841	2.2	1.9
C ₈ mim	0.54	887	1.5	1.5

Table 1. Experimental values of the molar conductivity $\Lambda_{\text{imp}}/\Lambda_{\text{NMR}}$ ratio, the B -parameter from the VFT conductivity dependence, as well as the cationic and anionic self-diffusion constants $D_{\text{NMR}+}$ and $D_{\text{NMR}-}$ for ILs of the 1-alkyl-3-methylimidazolium cation and TFSI anion.

¹³ Where N_A is the Avogadro number, e is the electric charge on each ionic carrier, k is the Boltzmann constant and T is the temperature.

4.3. Confocal μ -Raman spectroscopy: *In-situ* fuel cell diagnostic

A very informative way to investigate the transport properties within a PEM is by *in situ* confocal Raman spectroscopy. With this technique the state of the electrolyte can be resolved in both space and time and correlated to the overall performance of the PEM fuel cell in which it is operated. This technique was first demonstrated for an H_2/H_2 cell [49] and later further developed for a H_2/O_2 PEM fuel cell [50, 51], see also Figure 9A. Using the confocal set up, good quality Raman spectra can be recorded across the whole thickness of the PEM, from anode to cathode (or *vice versa*), with spatial intervals of a few μm . Provided transparency of the material to the visible and small refraction index mismatch (with respect to air), the loss in Raman intensity and spatial resolution at depth are negligible. Under these conditions, the user can diagnostic the state of both the membrane and the liquid phase (water in hydrated Nafion and IL in IL swelled membranes) varying the operational conditions such as temperature, relative humidity, gas pressure, *etc.* Thus, with this *in situ* technique, both the structural robustness of the membrane and transport phenomena can be investigated *operando*.

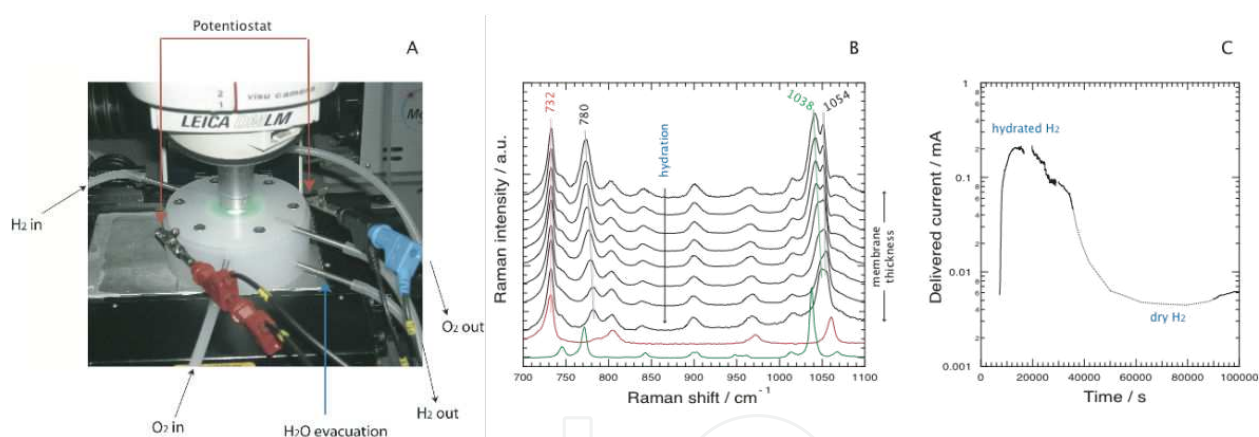


Figure 9. A: the fuel cell specially designed for *in situ* confocal μ -Raman measurements. B: a set of Raman spectra recorded during fuel cell operation from the H_2 (bottom) to the O_2 side (top), through the whole membrane's thickness. Spectra of a hydrated Nafion membrane (red) and of the IL (green) are also shown for comparison. C: plot of the current delivered by the fuel cell under varying degrees of hydration. The highest current delivered corresponds to the highest hydration level. These figures have been reproduced with permission from reference [50].

In reference [50] the authors demonstrate the potentiality of this technique through the study of a Nafion membrane swelled with protic ILs of the triethylammonium cation. In this particular case, the humidification of the H_2 gas was varied during fuel cell operation, whereby also the membrane became more or less hydrated. This *in situ* investigation showed that while the vibrational modes associated to the backbone of Nafion ($\nu_s CF_2$ at 732 cm^{-1}) remained unchanged at different hydration degrees, those due to $-SO_3^-$ groups (νSO_3

at 1038–1049 cm^{-1} for the IL's anion (in this specific case CH_3SO_3^-) and at 1050–1061 cm^{-1} (for the sulfonic acid group of Nafion) varied in frequency, Figure 9B.

The blue-shift of the νSO_3 (IL's anion) in the more hydrated state indicates a stronger association state, most probably to water molecules that are thought to find interstitial positions between cations and anions in $\text{H}_2\text{O}/\text{IL}$ mixtures, thus disrupting the original local organization. These features are of high relevance for fuel cell applications and deserve further investigations. The employment of *in situ* μ -Raman spectroscopy on operating fuel cell is one appropriate tool to understand the local dynamics and interactions around the protic species, putting these in relation to the overall performance of the PEM.

The authors also demonstrate that if the Raman spectra are correctly interpreted,¹⁴ possible concentration gradients of the IL induced by electro-osmotic drag across the membrane can also be resolved *operando*. From the quantitative analysis of Raman spectra, the authors also found that the membrane does not lose significant amounts of IL even after hydration cycles and four days of fuel cell operation. This is a very important result that supports the concept of IL swelled Nafion membranes for real fuel cell applications.

5. Conclusions

ILs are materials with an incredible variety of application fields. In this chapter, we have given examples of IL structures that can be used in fuel cells and Li-ion batteries, but use in super-capacitors, solar cells and green chemistry must not be forgotten. Very recently, ILs have also shown to have an important role in the extraction process of heavy metals from waste water. In all these applications, dynamical and structural properties jointly govern the functionality of ILs; yet in the field of ILs local structure and dynamics are rarely investigated in strict relation to each other. The combination of complementary experimental techniques like SAXS and pfg-NMR and the use of *in situ* spectroscopic methods are highly recommended for a better understanding of the real functionality of IL-derived materials, in particular those of interest for green energy applications. In this context, I foresee that *in situ* μ -Raman, *in situ* μ -NMR imaging and CP MAS NMR spectroscopy will be of increased importance in the next coming years.

Acknowledgements

The author acknowledges the financial support from the Chalmers' Areas of Advance Energy and Materials Science, as well as the Swedish Foundation for Strategic Research (SSF). Dr. M. Maréchal is also acknowledged for fruitful scientific discussions on the use (and interpretation) of SAXS in ionic liquids. A special thank goes also to all my previous and current collaborators.

¹⁴ Through calibrated relative intensity curves.

Author details

Anna Martinelli

Address all correspondence to: anna.martinelli@chalmers.se

Applied Surface Chemistry, Department of Chemical and Biological Engineering, Chalmers University of Technology, Gothenburg, Sweden

References

- [1] Walden P., Bull. Acad. Imper. Sci. (St. Petersburg) 1914; 8: 405–422.
- [2] Wasserscheid P., Keim W. Ionic liquids – New ‘solutions’ for transition metal catalysis. *Angewandte Chemie - International Edition* 2000; 39(21): 3773–3789.
- [3] Wilkes J.S. A short history of ionic liquids - from molten salts to neoteric solvents. *Green Chemistry* 2002; 4: 73–80.
- [4] Ohno H., editor, *Ionic Liquids: The Front and Future of Material Developments*. CMC, Tokyo; 2003.
- [5] Armand M. Ionic-liquid materials for the electrochemical challenges of the future. *Nature Materials* 2009; 8(8): 621–629.
- [6] Goyal R.K., Jayakumar N.S., Hashim M.A. Emulsion stabilization using ionic liquid [BMIM]⁺[NTf₂]⁻ and performance evaluation on the extraction of chromium. *Journal of Hazardous Materials* 2011; 195: 55–61.
- [7] Tokuda H., Ishii K., Susan M.A.B.H., Tsuzuki S., Hayamizu K., Watanabe M.. Physicochemical properties and structures of room-temperature ionic liquids. 3. Variation of cationic structures. *Journal of Physical Chemistry B* 2006; 110(6): 2833–2839.
- [8] Hirao M., Sugimoto H., Ohno H. Preparation of novel room-temperature molten salts by neutralization of amines. *Journal of The Electrochemical Society* 2000; 147(11): 4168–4172.
- [9] Yoshizawa M., Xu M., Angell C.A. Ionic Liquids by Proton Transfer: Vapor Pressure, Conductivity, and the Relevance of ΔpK_a from Aqueous Solutions. *Journal of the American Chemical Society* 2003; 125(50): 15411–15419.
- [10] Tokuda H., Hayamizu K., Ishii K., Susan M.A.B.H., Watanabe M. Physicochemical properties and structures of room temperature ionic liquids. 2. Variation of alkyl chain length in imidazolium cation. *Journal of Physical Chemistry B* 2005; 109(13): 6103–6110.

- [11] Tokuda H., Hayamizu K., Ishii K., Susan Md.A.B.H., Watanabe M. Physicochemical properties and structures of room temperature ionic liquids. 1. Variation of anionic species. *Journal of Physical Chemistry B* 2004; 108(42): 16593–16600.
- [12] Hagiwara R., Lee J.S. Ionic liquids for electrochemical devices. *Electrochemistry* 2007; 75(1): 23–34.
- [13] Kreuer K. D. On the development of proton conducting polymer membranes for hydrogen and methanol fuel cells. *Journal of Membrane Science* 2001; 185(1): 29–39.
- [14] Martinelli A., Matic A., Jacobsson P., Börjesson L., Navarra M.A., Panero S., Scrosati B. A structural study on ionic-liquid-based polymer electrolyte membranes. *Journal of the Electrochemical Society* 2007; 154(8): G183–G187.
- [15] Martinelli A., Matic A., Jacobsson P., Börjesson L., Fericola A., Panero S., Scrosati B., Ohno H., Physical properties of proton conducting membranes based on a protic ionic liquid. *Journal of Physical Chemistry B* 2007; 111 (43): 12462–12467.
- [16] Iojoiu C., Martinez M., Hanna M., Molmeret Y., Cointeaux L., Leprêtre J.-C., El Kissi N., Sanchez J.-Y. PILs-based Nafion membranes: A route to high-temperature PEFMCs dedicated to electric and hybrid vehicles. *Polymers for Advanced Technologies* 2008; 19(10): 1406–1414.
- [17] Judeinstein P., Iojoiu C., Sanchez J.-Y., Ancian B. Proton conducting ionic liquid organization as probed by NMR: self-diffusion coefficients and heteronuclear correlations. *Journal of Physical Chemistry B* 2008; 112(12): 3680–3683.
- [18] Lazzari M., Scrosati B. A Cyclable Lithium Organic Cell Based on Two Intercalation Electrodes. *Journal of the Electrochemical Society* 1980; 127(3): 773–774.
- [19] Fericola A., Croce F., Scrosati B., Watanabe M., Ohno H. LiTFSI-BEPyTFSI as an improved ionic liquid electrolyte for rechargeable lithium batteries. *Journal of Power Sources* 2007; 174(1): 342–348.
- [20] Shimano S., Zhou H., Honma I. Preparation of nanohybrid solid-state electrolytes with liquid like mobilities by solidifying ionic liquids with silica particles. *Chemistry of Materials* 2007; 19(22): 5216–5221.
- [21] Ueno K., Hata K., Katakabe T., Kondoh M., Watanabe M. Nanocomposite ion gels based on silica nanoparticles and an ionic liquid: ionic transport, viscoelastic properties, and microstructure. *Journal of Physical Chemistry B* 2008; 112(30): 9013–9019.
- [22] Sharp K.G. A two-component, non-aqueous route to silica gel. *Journal of Sol-Gel Science and Technology* 1994; 2(1-3): 35–41.
- [23] Néouze M.-A., Le Bideau J., Gaveau P., Bellayer S., Vioux A. Ionogels, new materials arising from the confinement of ionic liquids within silica-derived networks. *Chemistry of Materials* 2006; 18(17): 3931–3936.

- [24] Le Bideau J., Gaveau P., Bellayer S., Néouze M.-A., Vioux A. Effect of confinement on ionic liquids dynamics in monolithic silica ionogels: ^1H NMR study. *Physical Chemistry Chemical Physics* 2007; 9(40): 5419–5422.
- [25] Martinelli A., Nordstierna L. An investigation of the sol-gel process in ionic liquid-silica gels by time resolved Raman and ^1H NMR spectroscopy. *Physical Chemistry Chemical Physics* 2012; 14(38): 13216–13223.
- [26] Nayeri M., Martinelli A. Simultaneous Raman and SAXS investigation of the sol-gel process in ionogels of the 1-hexyl-3-methylimidazolium bis(trifluoromethanesulfonyl)imide ionic liquid. In manuscript; 2012.
- [27] Hayashi K. *Journal of The Electrochemical Society*, 2002; 202nd Meeting, Abstracts, MA 2002-2, No. 205.
- [28] Pitawala J., Kim J.-K., Jacobsson P., Koch V., Croce F., Matic A. Phase behaviour, transport properties, and interactions in Li-salt doped ionic liquids. *Faraday Discussions* 2012; 154: 71–78.
- [29] Martinelli A., Matic A., Johansson P., Jacobsson P., Börjesson L., Fernicola A., Panero S., Scrosati B., Ohno H. Conformational evolution of TFSI⁻ in protic and aprotic ionic liquids. *Journal of Raman Spectroscopy* 2011; 42(3): 522–528.
- [30] Chalmers J.M. and Griffiths P.R. *Handbook of Vibrational Spectroscopy; Theory and Instrumentation* (John Wiley and Sons, 2002).
- [31] Herstedt M., Smirnov M., Johansson P., Chami M., Grondin J., Servant L., Lassègues J.C. Spectroscopic characterization of the conformational states of the bis(trifluoromethanesulfonyl)imide anion (TFSI⁻). *Journal of Raman Spectroscopy* 2005; 36(8): 762–770.
- [32] Holbrey J.D., Reichert W.M., Rogers R.D. Crystal structures of imidazolium bis(trifluoromethanesulfonyl)imide 'ionic liquid' salts: The first organic salt with a cis-TFSI anion conformation. *Dalton Transactions* 2004; (15): 2267–2271.
- [33] Holomb R., Martinelli A., Albinsson I., Lassègues J.C., Johansson P., Jacobsson P. Ionic liquid structure: The conformational isomerism in 1-butyl-3-methyl-imidazolium tetrafluoroborate ([bmim][BF₄]). *Journal of Raman Spectroscopy* 2008; 39(7): 793–805.
- [34] Triolo A., Russina O., Bleiff H.-J., Di Cola E. Nanoscale segregation in room temperature ionic liquids. *Journal of Physical Chemistry B* 2007; 111(18): 4641–4644.
- [35] Pott T., Méléard P. New insight into the nanostructure of ionic liquids: A small angle X-ray scattering (SAXS) study on liquid tri-alkyl-methyl-ammonium bis(trifluoromethanesulfonyl)amides and their mixtures. *Physical Chemistry Chemical Physics* 2009; 11(26): 5469–5475.
- [36] Triolo A., Russina O., Fazio B., Triolo R., Di Cola E. Morphology of 1-alkyl-3-methylimidazolium hexafluorophosphate room temperature ionic liquids. *Chemical Physics Letters* 2008; 457(4-6): 362–365.

- [37] Martinelli A., Maréchal M., Åsa Östlund. Correlation between molecular structure and transport properties in 1-alkyl-3-methylimidazolium ionic liquids: a combined pfg-NMR and X-ray scattering study. In manuscript 2012.
- [38] Russina O., Triolo A. New experimental evidence supporting the mesoscopic segregation model in room temperature ionic liquids. *Faraday Discussions* 2012; 154: 97–109.
- [39] Hardacre C., Holbrey J.D., Mullan C.L., Youngs T.G.A., Bowron D.T. Small angle neutron scattering from 1-alkyl-3-methylimidazolium hexafluorophosphate ionic liquids ([Cnmim] [PF₆], n=4, 6, and 8). *Journal of Chemical Physics* 2010; 133(7): 074510-074517.
- [40] Kremer F. and Schonhals A., editors. *Broadband Dielectric Spectroscopy*. Springer-Verlag; 2003.
- [41] Hohne G., Hemminger W. and Flammersheim H.-J., editors. *Differential Scanning Calorimetry*. Springer-Verlag; 1996.
- [42] Martinelli A., Matic A., Jacobsson P., Börjesson L., Fericola A., Scrosati B. Phase behavior and ionic conductivity in lithium bis(trifluoromethanesulfonyl)imide-doped ionic liquids of the pyrrolidinium cation and bis(trifluoromethanesulfonyl)imide anion. *Journal of Physical Chemistry B* 2009; 113(32): 11247–11251.
- [43] Pitawala J., Matic A., Martinelli A., Jacobsson P., Koch V., Croce F. Thermal properties and ionic conductivity of imidazolium bis(trifluoromethanesulfonyl)imide dicationic ionic liquids. *Journal of Physical Chemistry B* 2009; 113(32): 10607–10610.
- [44] Price W.S. Pulsed-field gradient nuclear magnetic resonance as a tool for studying translational diffusion: Part 1. Basic theory. *Concepts in Magnetic Resonance* 1997; 9(5): 299–335.
- [45] Tokuda H., Tsuzuki S., Susan M.A.B.H., Hayamizu K., Watanabe M. How ionic are ionic liquids? An indicator of the physicochemical properties. *Journal of Physical Chemistry B* 2006; 110(39): 19593–19600.
- [46] Noda A., Hayamizu K., Watanabe M. Pulsed-gradient spin-echo ¹H and ¹⁹F NMR ionic diffusion coefficient, viscosity, and ionic conductivity of non-chloroaluminate room-temperature ionic liquids. *Journal of Physical Chemistry B* 2001; 105(20): 4603–4610.
- [47] Kanakubo M., Harris K.R., Tsuchihashi N, Ibuki K., Ueno M. Effect of pressure on transport properties of the ionic liquid 1-butyl-3-methylimidazolium hexafluorophosphate. *Journal of Physical Chemistry B* 2007; 111(8): 2062–2069.
- [48] Liu H., Maginn E. A molecular dynamics investigation of the structural and dynamic properties of the ionic liquid 1-n-butyl-3-methylimidazolium bis(trifluoromethanesulfonyl) imide. *Journal of Chemical Physics* 2011; 135(12): 124507–16.

- [49] Matic H., Lundblad A., Lindbergh G., Jacobsson P. In situ micro-Raman on the membrane in a working PEM cell. *Electrochemical and Solid-State Letters* 2005; 8(1): A5–A7.
- [50] Martinelli A., Iojoiu C., Sergent N. A H₂/O₂ fuel cell for in situ -Raman measurements. In-depth characterization of an ionic liquid filled Nafion membrane. *Fuel Cells* 2011; 12(2): 169–178.
- [51] Huguet P., Morin A., Gebel G., Deabate S., Sutor A.K., Peng Z. In situ analysis of water management in operating fuel cells by confocal Raman spectroscopy. *Electrochemistry Communications* 2011; 13(5): 418–422.

IntechOpen